



Article

Nucleosome Assembly Protein 1, Nap1, Is Required for the Growth, Development, and Pathogenicity of *Magnaporthe oryzae*

Qing Wang¹, Jing Wang¹, Pengyun Huang¹, Zhicheng Huang¹, Yan Li¹, Xiaohong Liu² , Fucheng Lin^{2,3} and Jianping Lu^{1,*}

- ¹ State Key Laboratory for Managing Biotic and Chemical Threats to the Quality and Safety of Agro-Products, College of Life Sciences, Zhejiang University, Hangzhou 310058, China; m15760206862_1@163.com (Q.W.); wj9311@163.com (J.W.); huangpengyun2012@163.com (P.H.); huangzhicheng1210@163.com (Z.H.); leeysmailbox@163.com (Y.L.)
- ² Institute of Biotechnology, Zhejiang University, Hangzhou 310058, China; xhliu@zju.edu.cn (X.L.); fuchenglin@zju.edu.cn (F.L.)
- ³ State Key Laboratory for Managing Biotic and Chemical Threats to the Quality and Safety of Agro-Products, Institute of Plant Protection and Microbiology, Zhejiang Academy of Agricultural Sciences, Hangzhou 310021, China
- * Correspondence: jplu@zju.edu.cn

Abstract: *Magnaporthe oryzae* is the causal agent of rice blast, leading to significant reductions in rice and wheat productivity. Nap1 is a conserved protein in eukaryotes involved in diverse physiological processes, such as nucleosome assembly, histone shuttling between the nucleus and cytoplasm, transcriptional regulation, and the cell cycle. Here, we identified Nap1 and characterized its roles in fungal development and virulence in *M. oryzae*. MoNap1 is involved in aerial hyphal and conidiophore differentiation, sporulation, appressorium formation, plant penetration, and virulence. Δ MoNap1 generated a small, elongated, and malformed appressorium with an abnormally organized septin ring on hydrophobic surfaces. Δ MoNap1 was more sensitive to cell wall integrity stresses but more resistant to microtubule stresses. MoNap1 interacted with histones H₂A and H₂B and the B-type cyclin (Cyc1). Moreover, a nuclear export signal (NES) domain is necessary for Nap1's roles in the regulation of the growth and pathogenicity of *M. oryzae*. In summary, NAP1 is essential for the growth, appressorium formation, and pathogenicity of *M. oryzae*.

Keywords: rice blast; virulence; septin ring; cell wall integrity; histone; appressorium



Citation: Wang, Q.; Wang, J.; Huang, P.; Huang, Z.; Li, Y.; Liu, X.; Lin, F.; Lu, J. Nucleosome Assembly Protein 1, Nap1, Is Required for the Growth, Development, and Pathogenicity of *Magnaporthe oryzae*. *Int. J. Mol. Sci.* **2022**, *23*, 7662. <https://doi.org/10.3390/ijms23147662>

Academic Editor: Sixue Chen

Received: 25 May 2022

Accepted: 8 July 2022

Published: 11 July 2022

Publisher's Note: MDPI stays neutral with regard to jurisdictional claims in published maps and institutional affiliations.



Copyright: © 2022 by the authors. Licensee MDPI, Basel, Switzerland. This article is an open access article distributed under the terms and conditions of the Creative Commons Attribution (CC BY) license (<https://creativecommons.org/licenses/by/4.0/>).

1. Introduction

Magnaporthe oryzae (syn. *Pyricularia oryzae*)-induced rice blast is a highly destructive rice disease capable of causing massive yield reductions in rice or wheat crops worldwide [1]. At the beginning of infection, a three-celled conidium adheres to the rice surface, germinates under suitable conditions (appropriate temperature and humidity), and forms a germ tube, which subsequently differentiates into a melanized, dome-shaped appressorium stimulated by external hydrophobic signals and hardness [2,3]. During appressorium maturation, the glycogen granules and lipid droplets in conidia are gradually degraded and translocated to appressoria, resulting in the accumulation of a high concentration of glycerol, which generates a turgor pressure of up to 8 MPa [4]. The immense turgor provokes great mechanical pressure in an appressorium and promotes its further development into a penetration peg that quickly develops into invasive hyphae in plant cells. After approximately 5–7 days, the typical necrotic spots of rice blast appear on plant surfaces. At this time, a large number of secondary conidia are released from conidial stalks, and start the next round of the infection cycle [5].

Nap1, nucleosome assembly protein 1, was first identified in HeLa cell extracts due to its function in stimulating nucleosome assembly [6]. Nap1 is conserved in eukaryotes

and plays diverse biological roles, such as in yeast, *Xenopus*, *Drosophila* [7], *Arabidopsis thaliana* [8], and soybean [9]. In *Drosophila melanogaster*, the deletion of *NAP1* greatly reduces viability [10]. In mice, Nap1 belongs to a multigene family, and the knockout of the neuron-specific *NAP1-homolog-2* gene is embryo lethal [11]. In plants, Nap1 also belongs to a multigene family, and different Nap1 members in tobacco (*Nicotiana tabacum*) and rice (*Oryza sativa*) have different subcellular localizations and appear to perform specific functions [12].

In the nucleosome assembly, Nap1 directly binds core histones and transfers them to naked DNA [13]. In histones, Nap1 has higher affinity levels for binding H₂A and H₂B than H3 and H4 in vitro [14]. In *Saccharomyces cerevisiae*, the deletion of *NAP1* led to defects in nucleosome assembly and altered the expression of approximately 10% of nuclear genes [15]. In addition to the nucleosome assembly, Nap1 is involved in the cell cycle [16], histone shuttling between the nucleus and cytoplasm [17], microtubule dynamics and septin assembly [18]. In *S. cerevisiae*, Nap1 was found to bind B-type cyclin 2 (Clb2) and participate in mitosis by regulating Clb2/p34^{CDC28} kinase activity [19]. The protein kinase Gin4 is specifically activated during mitosis, and the phosphorylation and activation of Gin4 during mitosis depend on Clb2 and Nap1 [16]. In animals and yeasts, the dynamic shuttling of Nap1 and Nap1-like proteins between the cytoplasm and nucleus is important for the cell cycle [20]. In *Drosophila* embryonic cells, Nap1 is localized in the nucleus during the S phase and significantly in the cytoplasm during the G2 phase [21]. Similarly, human Nap1L4 appears in the nucleus only during the S phase [22]. Nap1 contains a series of evolutionarily conserved structural domains and motifs, including a nuclear localization signal (NLS) [21], a nuclear export signal (NES) [7], and an acidic segment at the C-terminus that is functionally dispensable for promoting nucleosome assembly [23]. When a nuclear export sequence (NES) is deleted, yeast Nap1 appears to localize in the nucleus [20]. A crystal structure analysis revealed that the NES sequence is covered by a domain that harbors several casein kinase 2 (CK2) phosphorylation sites. The cell cycle-dependent location of Nap1 proteins seems to depend on its phosphorylation state, which is controlled by CK2 [24]. Moreover, Nap1 may have a direct effect on microtubule dynamics. In particular, *NAP1*-deficient yeast cells are resistant to benomyl, a drug that destabilizes microtubules [19]. These data suggest that Nap1 is certainly a multifunctional protein that performs functions in both the nucleus and the cytoplasm.

The function of Nap1 in *M. oryzae* and other pathogenic fungi is not well understood. In this study, we identified the biological functions of Nap1 in *M. oryzae* through gene knockout and phenotypic analyses. We confirmed that MoNap1 interacted with histones H₂A and H₂B and a B-type cyclin (Cyc1). However, MoNap1 was primarily localized in the cytoplasm, and the NES domain of MoNap1 was dispensable for localization but necessary for its roles in growth and virulence. Overall, we found that *NAP1* played indispensable roles in regulating the growth, sporulation, appressorium formation, and pathogenicity of *M. oryzae*.

2. Results

2.1. Identification and Targeted Gene Deletion of *NAP1* in *M. oryzae*

Nucleosome assembly protein 1 in *M. oryzae*, Nap1 (MGG_06924/XP_003709662), was identified by searching for proteins homologous to *S. cerevisiae* Nap1 in the rice blast genome. MoNap1 contains a 404-amino acid polypeptide that shares 45.99% sequence identity with *S. cerevisiae* Nap1 [7]. A phylogenetic tree was constructed based on the amino acid sequences of nucleosome assembly proteins in several species, including *S. cerevisiae* [25], *D. melanogaster* [24], *Homo sapiens* [26], *Candida albicans* [18], *Schizosaccharomyces pombe* [27], *Aspergillus clavatus*, *Aspergillus flavus*, *Aspergillus melleus*, *Neosartorya fischeri*, *Neosartorya fumigata*, and *Fusarium oxysporum*. The alignment tree showed that Nap1 of *M. oryzae* was more homologous to Nap1 of the filamentous fungus *F. oxysporum* than to those of *S. cerevisiae*, *C. albicans*, and *H. sapiens* (Figure 1).

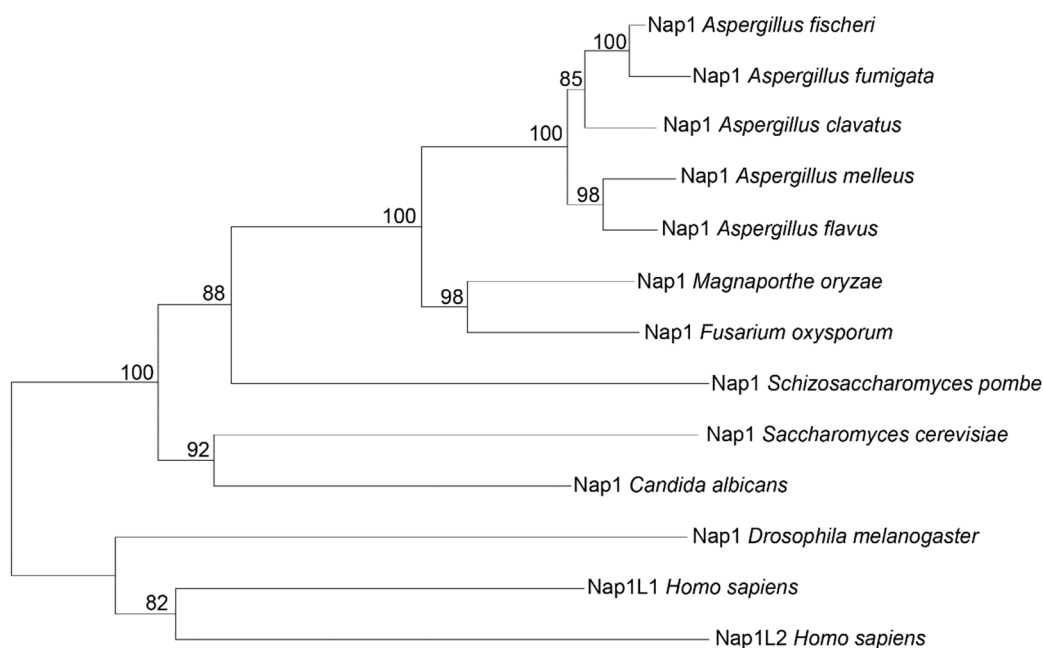


Figure 1. Nap1s are conserved in eukaryotes. Alignment tree of MoNap1 and Nap1 in *S. cerevisiae* (NP_012974.1), *Drosophila melanogaster* (NP_477128.1), *Homo sapiens* (XP_016874829.1, NP_068798.1), *Candida albicans* (XP_718658.1), *Schizosaccharomyces pombe* (NP_587838.1), *Aspergillus melleus* (XP_045950078.1), *Aspergillus clavatus* (XP_001273890.1), *Aspergillus fischeri* (XP_001266074.1), *Aspergillus flavus* (QRD88693.1), *Aspergillus fumigatus* (XP_754077.1), and *Fusarium oxysporum* (XP_031048533.1).

Using the gene replacement strategy, we knocked out *NAP1* in the wild-type *M. oryzae* strain 70-15 (Figure S1A). We verified that the insertion copy number of *HPH* into Δ *Monap1* mutant genome was single by qPCR (Table S1). Based on Δ *Monap1*, we characterized the role of *NAP1* in the growth and pathogenicity of *M. oryzae*. To determine whether the mutant phenotype is caused by the deletion of *MoNAP1*, we built a complementation strain of Δ *Monap1* (*Monap1c*) by transforming the full-length genomic copy of *MoNAP1* into Δ *Monap1*. We also complemented Δ *Monap1* with the *NAP1* gene of *S. cerevisiae* (*Ynap1c*) (Figure S1B–F). In the following section, we describe the biological function of MoNap1 in detail.

2.2. *NAP1* Is Involved in Sporulation and Appressorium Formation in *M. oryzae*

The Δ *Monap1* mutant grew more slowly than the wild type 70-15 in CM, exhibiting reductions in mycelial growth of approximately 20%. The colony diameter of Δ *Monap1* was 4.24 ± 0.04 cm, while that of the wild type was 5.18 ± 0.02 cm at 9 dpi (days post inoculation) (Figure 2A,B). In addition, the colonies of the mutant appeared thinner and whiter than those of the wild type (Figure 2A). Δ *Monap1* is more susceptible to senescence, which can be observed by the collapse and autolysis of the aerial hyphae at the center of the colony (Figure 2A), indicating that MoNap1 may play a role in the aging process. However, the growth of Δ *Monap1* in MM was comparable to that of the wild type 70-15 (Figure 2C,D). Δ *Monap1* produced significantly fewer spores, approximately 1/8 of the wild type (Figure 2E). In Δ *Monap1*, the mRNA levels of two transcription factor genes *FLBC* and *CON7*, which are involved in the regulation of sporulation, were significantly downregulated (Figure S2). In the wild type, many conidiophores bearing spores in a typical sympodial mode were observed, while Δ *Monap1* produced fewer conidiophores and fewer spores in each conidiophore (Figure 2F). The appressorial morphology of Δ *Monap1* was distorted. The appressoria of the wild type were usually circular or dome-shaped, while approximately $61.5 \pm 11.4\%$ of the appressoria in Δ *Monap1* were abnormal (Figure 3A,B) and smaller than those in the wild type (the diameter of appressoria in the wild type was

11.86 ± 0.34 μm, whereas that in the $\Delta Monap1$ mutant was 8.98 ± 0.07 μm) (Figure 3C). The germ tubes of the $\Delta Monap1$ mutants were significantly longer than those of the wild type when germinated on hydrophobic plastic coverslips (Figure 3A,D). The germ tube of the wild type was 16.04 ± 1.55 μm in length, whereas that of $\Delta Monap1$ was 57.89 ± 7.07 μm (Figure 3D). Spore germination was not affected by the *MoNAP1* deletion at 4 hpi (hours post inoculation); however, the appressorial formation rate in $\Delta Monap1$ was lower than that in the wild type at 24 hpi (89.8 ± 3.2% in $\Delta Monap1$ compared to 99.0 ± 0.7% in the wild type) (Figure 3E). In addition, turgor pressure of appressoria at 24 hpi was not significantly different between $\Delta Monap1$ mutants and wild-type (Figure S3).

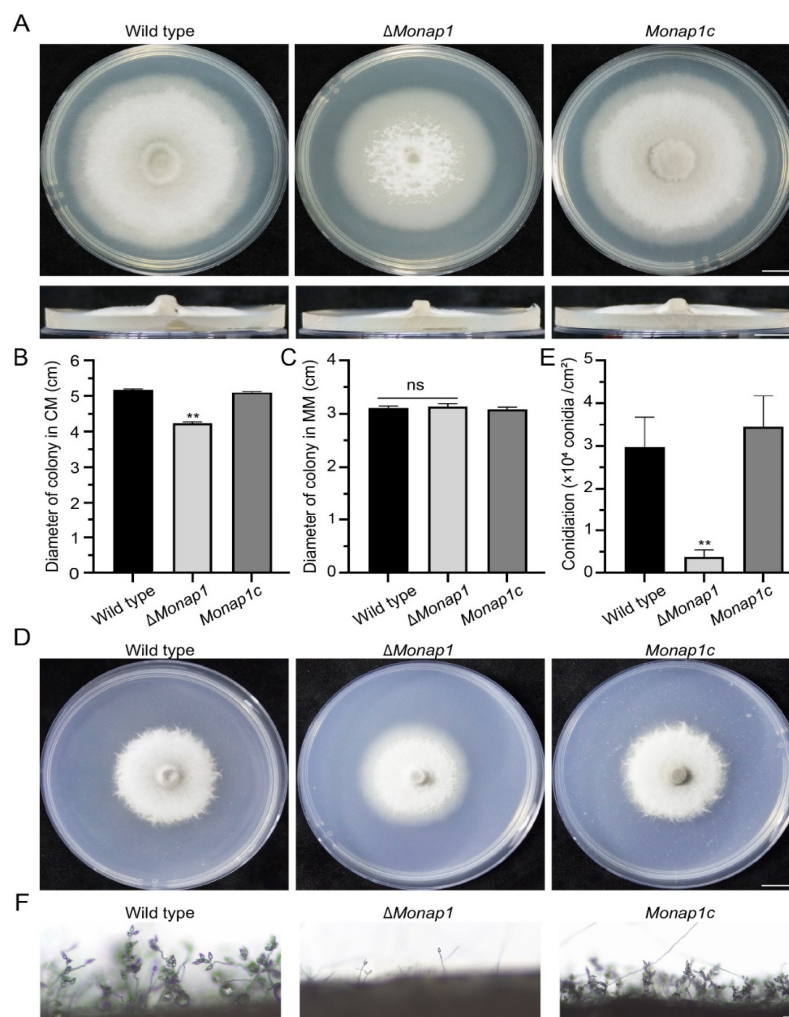


Figure 2. *NAP1* is required for the growth and conidiation of *M. royzae*. (A) Colonies of the wild-type, $\Delta Monap1$, and *MoNAP1* complemented strains of $\Delta Monap1$ (*Monap1c*). Bar, 1 cm. (B) Mycelial growth (cm) of the wild-type, $\Delta Monap1$ and *Monap1c* colonies in CM. $n = 5$ independent biological replicates. Error bars represent the standard deviations. The data were analyzed by GraphPad Prism 8.0 and significant differences compared with the wild type were estimated by multiple t tests: ** $p < 0.01$. (C) Mycelial growth (cm) of the wild type, $\Delta Monap1$ and *Monap1c* colonies in MM. $n = 5$ independent biological replicates. Error bars represent the standard deviations. The data were analyzed by GraphPad Prism 8.0 and significant differences compared with the wild type were estimated by multiple t tests: ns, $p > 0.05$. (D) Colonies of the wild type, $\Delta Monap1$, and *Monap1c* in MM. Bar, 1 cm. (E) Conidiation of the wild type, $\Delta Monap1$ and *Monap1c* strains in CM. $n = 5$ independent biological replicates. Error bars represent the standard deviations. The data were analyzed by GraphPad Prism 8.0 and significant differences compared with the wild type were estimated by multiple t tests: ** $p < 0.01$. (F) Conidiophore development of *M. royzae* strains. Bar, 50 μm.

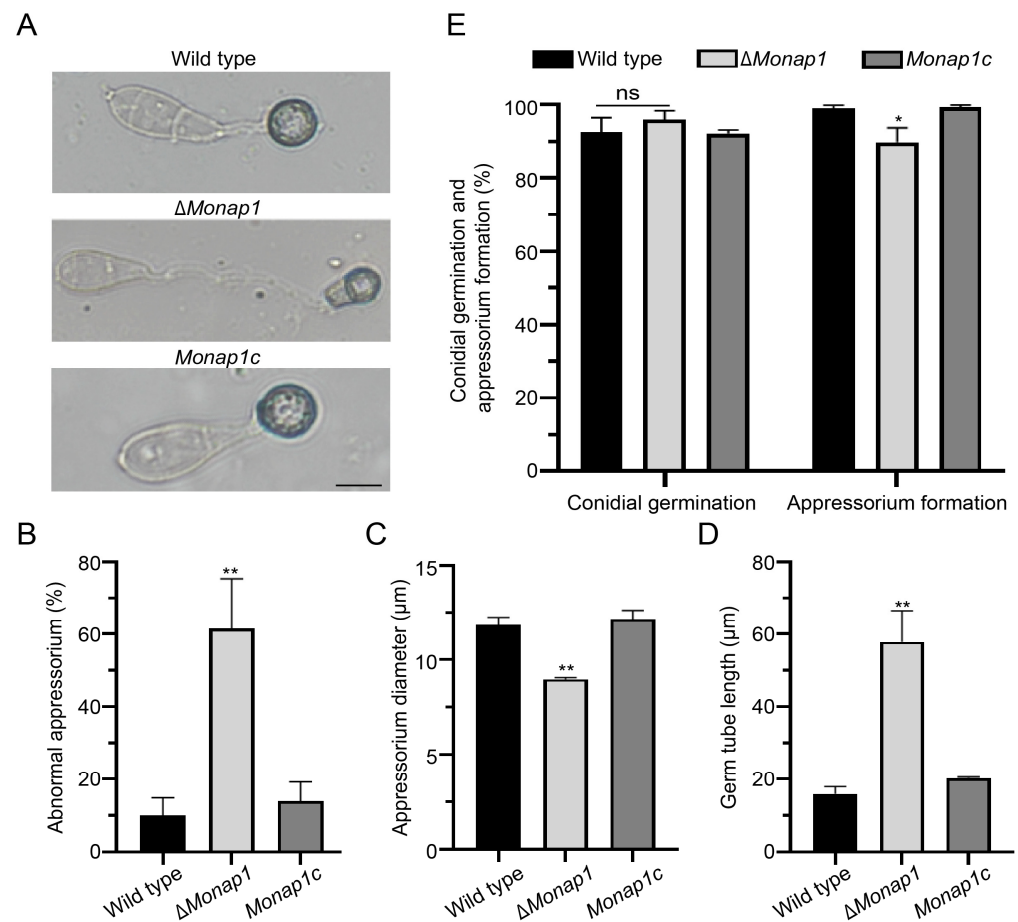


Figure 3. *NAP1* is required for appressorium formation. (A) Appressorium formation in the wild-type, $\Delta Monap1$ and *Monap1c* strains on hydrophobic surfaces at 24 hpi. Bar, 10 μm . (B) Abnormal appressoria rates (%) in the wild-type, $\Delta Monap1$ and *Monap1c* strains. At least 150 spores were counted per replicate. $n = 3$ independent biological replicates. Error bars represent the standard deviations. The data were analyzed by GraphPad Prism 8.0 and significant differences compared with the wild type were estimated by multiple t tests: ** $p < 0.01$. (C) The appressorium diameter in the wild-type, $\Delta Monap1$ and *Monap1c* strains at 24 hpi. At least 150 spores were counted per replicate. $n = 3$ independent biological replicates. Error bars represent the standard deviations. The data were analyzed by GraphPad Prism 8.0 and significant differences compared with the wild type were estimated by multiple t tests: ** $p < 0.01$. (D) Germ tube length (μm) in the wild-type, $\Delta Monap1$ and *Monap1c* strains. Approximately 100 appressoria were photographed and measured using the software NIS-Elements D 3.2 in triplicate. At least 150 spores were counted per replicate. $n = 3$ independent biological replicates. Error bars represent the standard deviations. The data were analyzed by GraphPad Prism 8.0 and significant differences compared with the wild type were estimated by multiple t tests: ** $p < 0.01$. (E) Conidial germination rate (%) at 4 hpi and appressorium formation rate (%) at 24 hpi in the wild-type, $\Delta Monap1$ and *Monap1c* strains. At least 150 spores were counted per replicate. $n = 3$ independent biological replicates. Error bars represent the standard deviations. The data were analyzed by GraphPad Prism 8.0 and significant differences compared with the wild type were estimated by multiple t tests: ns, $p > 0.05$, * $p < 0.05$.

The complementation strain *Monap1c* recovered the mutant's defects in mycelial growth, sporulation, conidiophore formation, and conidium differentiation, indicating that the defects in growth and conidiation of $\Delta Monap1$ were caused by the deletion of *NAP1*. We also complemented $\Delta Monap1$ with the *NAP1* gene of *S. cerevisiae* and found that *NAP1* in *S. cerevisiae* can restore the sporulation and virulence of the $\Delta Monap1$ mutant but not the growth of $\Delta Monap1$ (Figure 4A–D).

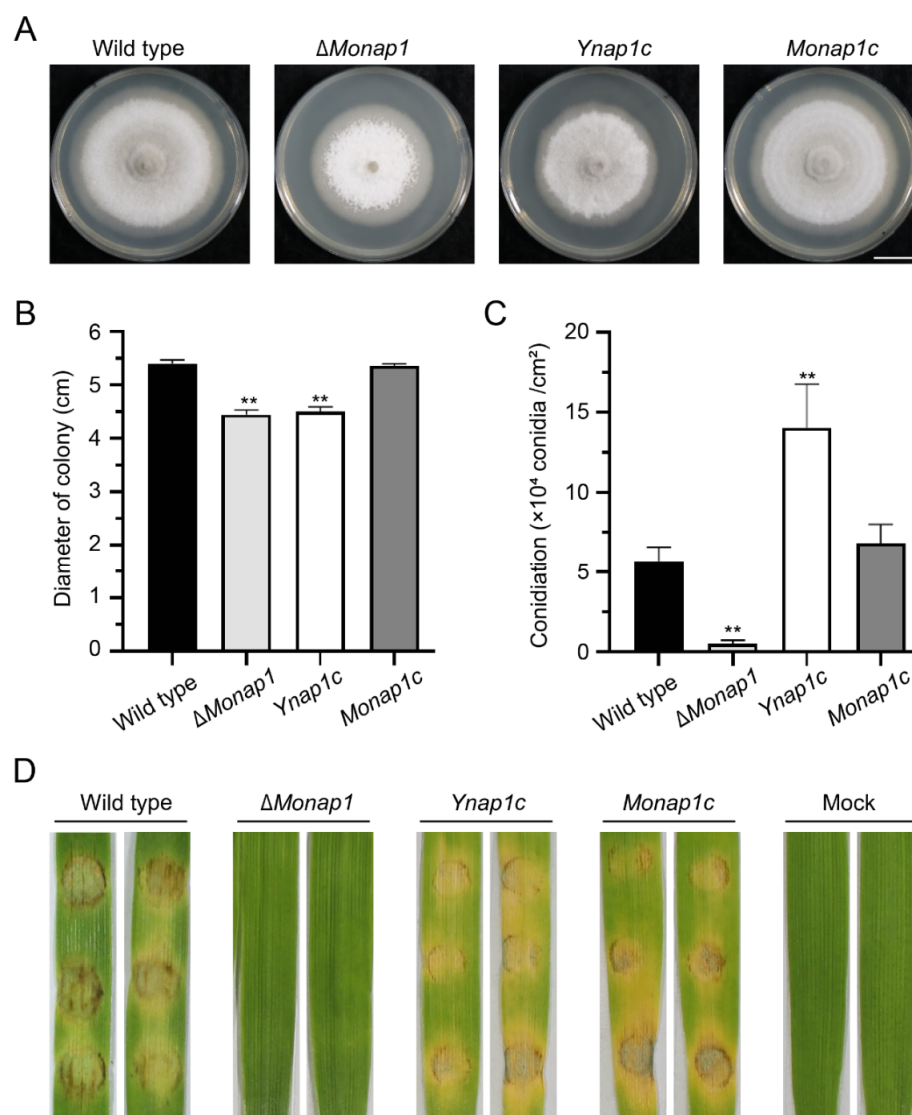


Figure 4. *NAP1* in *S. cerevisiae* can eliminate defects in the sporulation and virulence of Δ *Monap1*. (A) Colonies of the wild type, Δ *Monap1*, *NAP1* in *S. cerevisiae* complemented Δ *Monap1* strain (*Ynap1c*) and *Monap1c* strains. Bar, 1 cm. (B) Mycelial growth (cm) in the wild type, Δ *Monap1*, *Ynap1c*, and *Monap1c* strains. $n = 5$ independent biological replicates. Error bars represent the standard deviations. The data were analyzed by GraphPad Prism 8.0 and significant differences compared with the wild type were estimated by multiple *t* tests: ** $p < 0.01$. (C) Conidiation in the wild type, Δ *Monap1*, *Ynap1c*, and *Monap1c* strains. At least 150 spores were counted per replicate. $n = 3$ independent biological replicates. Error bars represent the standard deviations. The data were analyzed by GraphPad Prism 8.0 and significant differences compared with the wild type were estimated by multiple *t* tests: ** $p < 0.01$. (D) Disease symptoms on leaf explants of barley inoculated with mycelial plugs from wild type, Δ *Monap1*, *Ynap1c*, and *Monap1c*. The pictures were photographed at 4 dpi.

2.3. *NAP1* Is Required for Virulence in *M. oryzae*

The Δ *Monap1* mutant displayed reduced virulence on barley leaves and rice seedlings. We evaluated the fungal pathogenicity using three inoculation methods. At 4 dpi, the mycelial plugs of the wild-type 70-15 and the complementation strain *Monap1c* caused yellow and brown blast lesions and rotten plant tissues, while the mycelial plugs of Δ *Monap1* did not (Figure 5A). When inoculated on detached barley leaves with 20 μ L spore suspensions (5×10^4 conidia mL⁻¹) for 4 days, the disease lesions caused by Δ *Monap1* were apparently weaker than those caused by the wild type and the complementation strain

(Figure 5B). When sprayed on 2-week-old rice seedlings (CO-39) with conidial suspensions of 5×10^4 conidia mL^{-1} , the ΔMonap1 mutant caused small and restricted lesions in contrast to the typical spindle-like, gray centered, and merged blast lesions caused by the wild type and complementation strain at 7 dpi (Figure 5C). The lesion areas caused by ΔMonap1 were significantly lower than those caused by the wild type and *Monap1c* (those caused by ΔMonap1 were $19 \pm 8.1\%$, while those caused by the wild type and *Monap1c* were $52 \pm 4.6\%$ and $53 \pm 7.0\%$, respectively) (Figure 5D). Furthermore, we measured the penetration rate of the wild type, ΔMonap1 , and *Monap1c* at three time points (24 hpi, 36 hpi, and 48 hpi) (Figure 5E). At 24 hpi, 28.4 \pm 1.7% and 32.9 \pm 5.3% of appressoria penetrated into barley cuticle cells and formed invasive hyphae (IH) structures with the wild type and complementation strain *Monap1c*. However, only 3.1 \pm 1.8% of ΔMonap1 appressoria formed IH structures. At 36 hpi and 48 hpi, the appressorial penetration rate of ΔMonap1 was still lower than that of the wild type and the complementation strain *Monap1c* (Figure 5F). Moreover, the complemented ΔMonap1 with the *NAP1* gene of *S. cerevisiae* can restore the virulence of the ΔMonap1 mutant (Figure 4D).

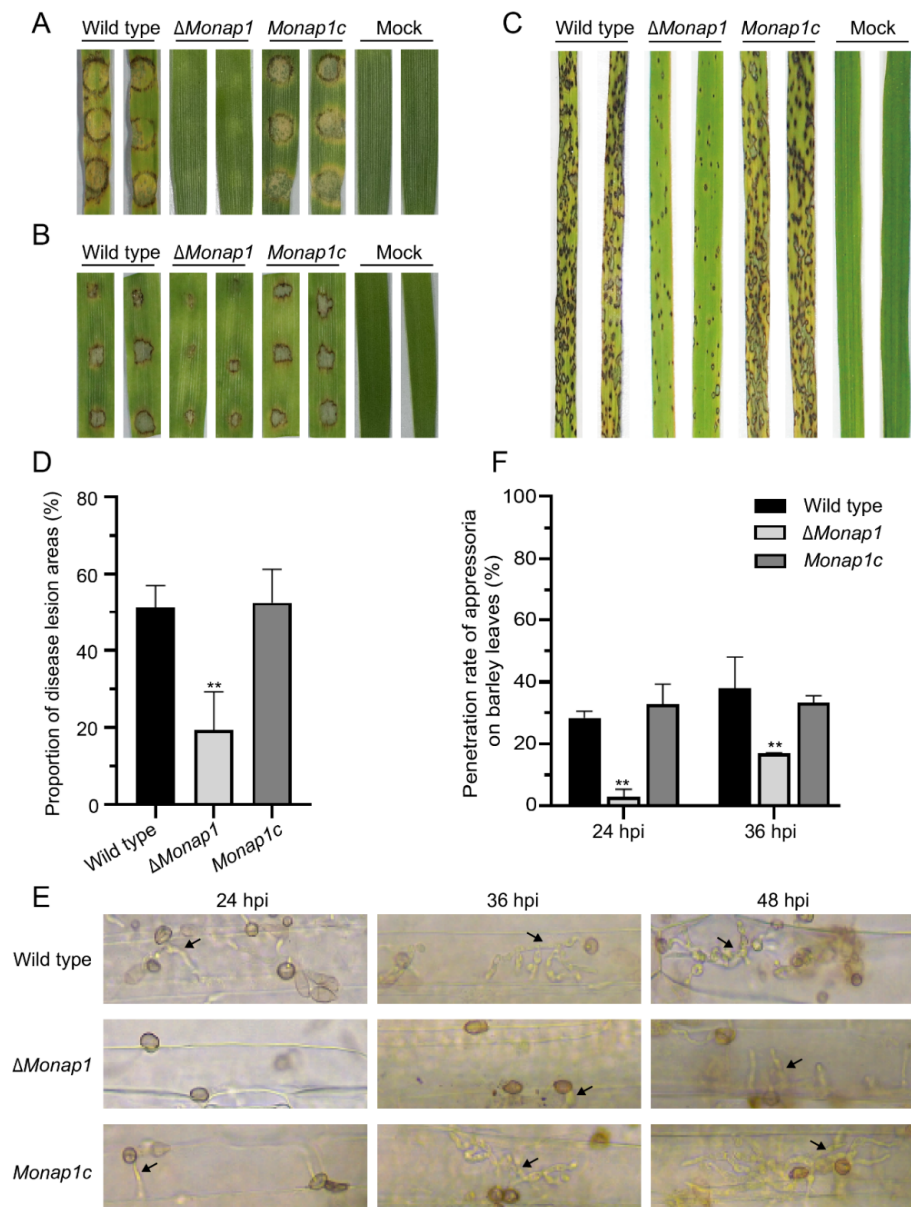


Figure 5. *NAP1* is required for virulence. (A) Disease symptoms of leaf explants of barley inoculated with mycelial plugs from the wild-type, ΔMonap1 and *Monap1c* strains. The pictures were photographed

at 4 dpi. (B) Disease symptoms of leaf explants of barley inoculated with spore suspensions (5×10^4 conidia mL^{-1}). (C) Two-week-old rice seedlings were inoculated by spraying 5×10^4 conidia mL^{-1} conidial suspensions from the wild type, ΔMonap1 and the complemented strain. Lesion severity on rice leaves was evaluated at 7 dpi. (D) The proportion of disease lesion areas (%) caused by the wild type, ΔMonap1 , and Monap1c strains on rice seedlings. The area occupied by disease spots per 5 cm of rice leaves was counted. At least 20 leaves were counted per replicate. $n = 3$ independent biological replicates. Error bars represent the standard deviations. The data were analyzed by GraphPad Prism 8.0 and significant differences compared with the wild type were estimated by multiple t tests: ** $p < 0.01$. (E) Invasive growth of *M. oryzae*. Barley leaf explants were inoculated with 20 μL of conidial suspension (5×10^4 conidia mL^{-1}) and cultured for 24 h, 36 h, and 48 h. The arrows indicate invasive hyphae. (F) Penetration rate (%) of the wild type, ΔMonap1 and Monap1c appressoria on barley leaves. At least 150 appressoria were counted per replicate. $n = 3$ independent biological replicates. Error bars represent the standard deviations. The data were analyzed by GraphPad Prism 8.0 and significant differences compared with the wild type were estimated by multiple t tests: ** $p < 0.01$.

2.4. ΔMonap1 Is Sensitive to Cell Wall Integrity Stresses and Resistant to Microtubule Stresses

The integrity of the cell wall, which is the first barrier contacting the external environment, plays a crucial role in the homeostasis of *M. oryzae* [28]. To assess the role of *MoNAP1* in cell wall integrity stress, the growth of the wild-type 70-15, ΔMonap1 and Monap1c strains was measured in CM with three cell wall integrity stresses, including 75 $\mu\text{g mL}^{-1}$ calcofluor white (CFW), 600 $\mu\text{g mL}^{-1}$ Congo red (CR), and 0.004% sodium dodecyl sulfate (SDS) (Figure 6A). The relative growth rate of mycelial growth of ΔMonap1 was significantly decreased compared to that of the wild type on CFW and CR (Figure 6B). In contrast, in the presence of 0.004% SDS, ΔMonap1 showed an increased relative growth rate compared to that of the wild type. In addition, ΔMonap1 was more resistant to bleomycin (BLM) than the wild type (Figure 6A,B).

In *S. cerevisiae*, the Δnap1 mutant showed increased resistance to benomyl, a microtubule destabilizing drug that causes mitotic arrest at high concentrations, suggesting that Nap1 plays a role in regulating microtubule dynamics [19]. Similar to yeast, the ΔMonap1 mutant grew faster than the wild type in plates containing 15 $\mu\text{g mL}^{-1}$ benomyl in *M. oryzae* (Figure 6A,B). In addition to benomyl, ΔMonap1 was more resistant to high temperature. ΔMonap1 exhibited a lower growth defect than the wild type at 32 °C (Figure 6A,B). When wild-type conidia are treated with HU, a DNA replication inhibitor, appressorium formation is blocked [29]. We inoculated wild-type 70-15, ΔMonap1 and Monap1c in CM containing 2 mM HU and found that ΔMonap1 had a higher relative growth rate than the wild type and Monap1c (Figure 6A,B).

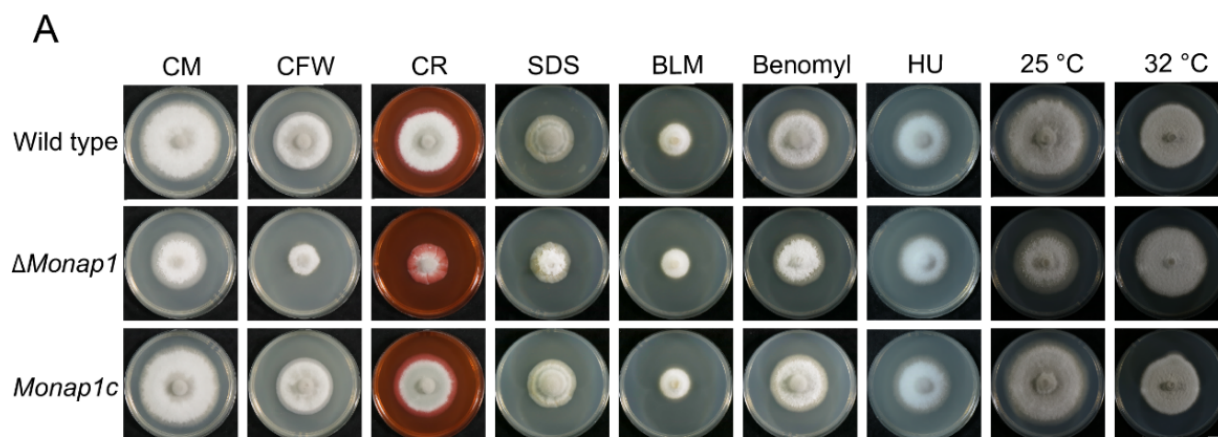


Figure 6. Cont.

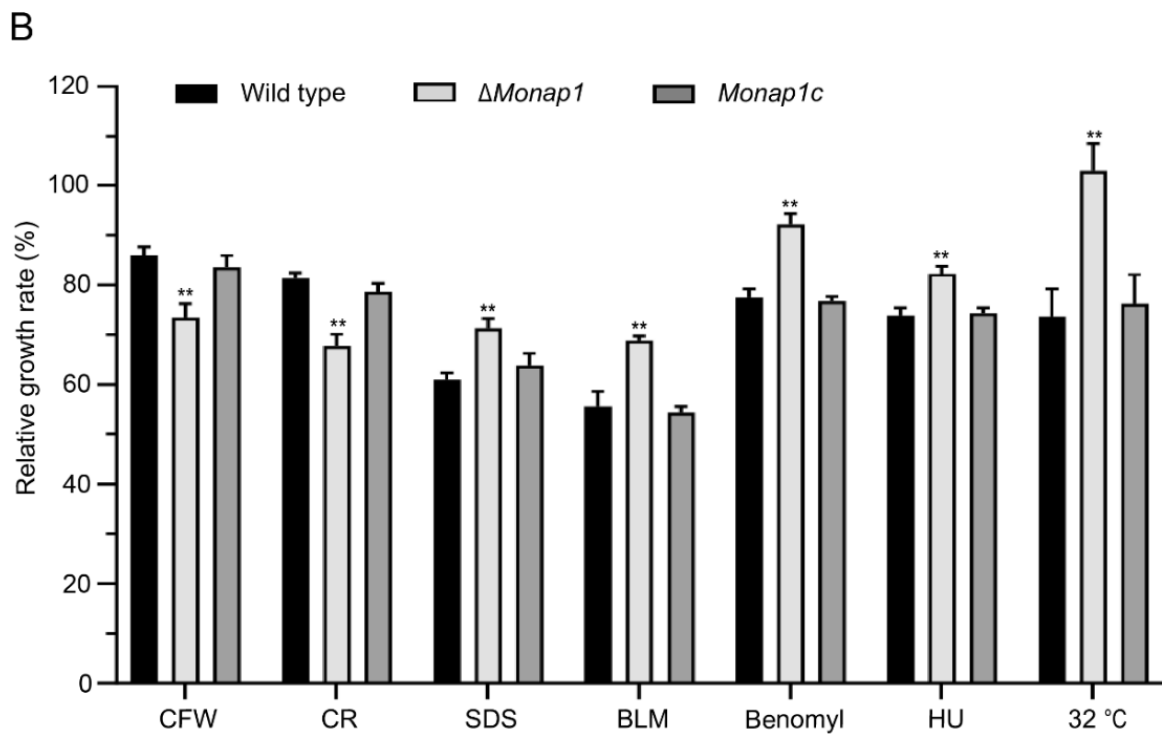


Figure 6. *MoNAP1* is involved in the cell wall integrity (CWI) pathway and microtubule dynamics. (A) Mycelial colonies of the wild type, $\Delta Monap1$ and *Monap1c* strains cultured in CM containing $75 \mu\text{g mL}^{-1}$ CFW, $600 \mu\text{g mL}^{-1}$ CR, 0.004% SDS, $35 \mu\text{g mL}^{-1}$ BLM, $15 \mu\text{g mL}^{-1}$ benomyl, and 2 mM HU in darkness at 25°C for 9 days. For the temperature-sensitivity assay, the wild type, $\Delta Monap1$ and *Monap1c* strains were cultured in CM at 25°C or 32°C under a 16 h light and 8 h dark cycle for 9 d. (B) Relative growth rate (%) of mycelial colonies in $75 \mu\text{g mL}^{-1}$ CFW, $600 \mu\text{g mL}^{-1}$ CR, 0.004% SDS and $35 \mu\text{g mL}^{-1}$ BLM, $15 \mu\text{g mL}^{-1}$ benomyl, 2 mM HU and 32°C growing conditions. $n = 5$ independent biological replicates. Error bars represent the standard deviations. The data were analyzed by GraphPad Prism 8.0 and significant differences compared with the wild type were estimated by multiple t tests: ** $p < 0.01$.

2.5. *Nap1* Is Necessary for Proper Septin Ring Organization in *M. oryzae*

A critical requirement for appressorium morphology and function in *M. oryzae* is the recruitment and organization of septin-dependent cytoskeletal components [30]. In *C. albicans*, *Nap1* plays a role in septin ring organization, and the deletion of *NAP1* affects the stability of the septin ring [18]. The abnormal appressorial morphology of $\Delta Monap1$ prompted us to observe the localization of the septin ring in the appressorium. We visualized the septin ring by expressing Sep3-GFP and Sep5-GFP fusion proteins in the wild type and mutants. In the wild type, Sep3-GFP and Sep5-GFP showed a ring structure around the appressorium pore, while in the $\Delta Monap1$ mutant, Sep3-GFP and Sep5-GFP were evenly distributed and appeared similar to a round pie at the bottom of the appressorium at 24 hpi (Figure 7).

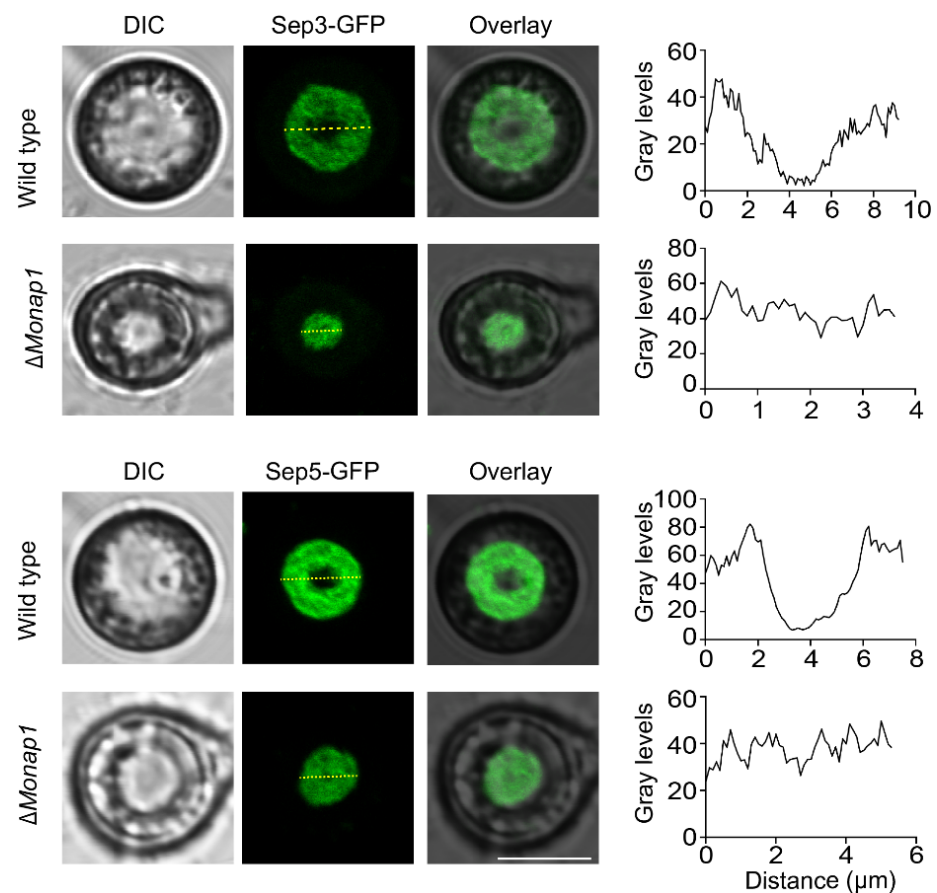


Figure 7. Δ Monap1 exhibits impaired septin organization. Expression of Sep3-GFP (upper panel) and Sep5-GFP (lower panel) in appressoria of *M. oryzae* in the wild type and Δ Monap1 mutant at 24 hpi. The septin ring showed aberrant distribution and organization in Δ Monap1. The distribution of the fluorescence signal in a transverse section (indicated by the yellow line) was analyzed by ImageJ software. Bar, 5 μ m.

2.6. Nap1 Binds Histones H₂A and H₂B and G2/Mitotic-Specific B-Type Cyclin Cyc1 in *M. oryzae*

As a nucleosome assembly protein, Nap1 can tightly bind histones H₂A and H₂B in yeast [31], *Drosophila* [21], and tobacco [32]. To characterize its biochemical properties in *M. oryzae*, we detected whether MoNap1 bound core histones. Using an in vitro GST pull-down assay, we identified the interaction between MoNap1 and histones H₂A and H₂B. The recombinant proteins GST-H₂A and GST-H₂B pulled down FLAG-MoNap1, but GST did not (Figure 8A). Furthermore, we detected in vivo protein interactions between MoNap1 and H₂A using a bimolecular fluorescence complementation (BiFC) assay. MoNap1 was fused to the C-terminal fragment of YFP (YFP^{CTF}), and H₂A was fused to the N-terminal fragment of YFP (YFP^{NTF}). The two vectors expressing MoNap1-YFP^{CTF} and YFP^{NTF}-H₂A were cotransformed into the wild type; as negative controls, MoNap1-YFP^{CTF} and YFP^{NTF} as well as YFP^{CTF} and YFP^{NTF}-H₂A were cotransformed into the wild type. Only transformants coexpressing MoNap1-YFP^{CTF} and YFP^{NTF}-H₂A showed YFP signals in the cytoplasm, but the transformants coexpressing two pairs of control vectors did not (Figure 8B).

In budding yeast, Nap1 acts with Clb2 to perform mitotic functions and suppress polar bud growth [19]. In *M. oryzae*, a B-type cyclin gene, *CYC1*, is the homolog of *CLB2* [33]. The different sensitivities of Δ MoNap1 to benomyl and temperature prompted us to investigate the relationship between Nap1 and the Cyc1 protein. In the pull-down experiments, MoNap1 was pulled down by Cyc1 (Figure 8C). Thus, MoNap1 physically interacted with Cyc1 in *M. oryzae*.

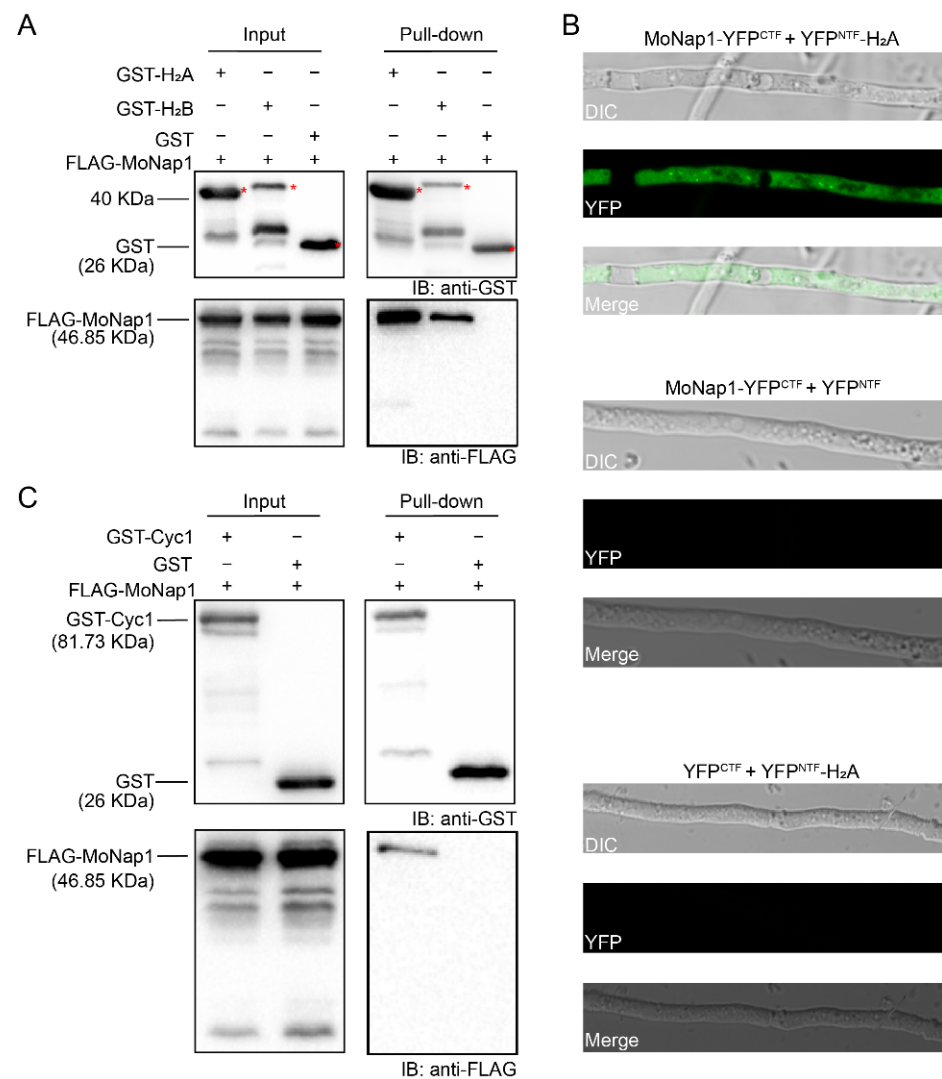


Figure 8. MoNap1 interacted with H₂A, H₂B, and Cyc1. (A) Pull-down results between FLAG-MoNap1 and GST-H₂A or GST-H₂B in *E. coli* BL21. FLAG-MoNap1 was detected in GST-H₂A and GST-H₂B eluents but not in GST eluents. Asterisks represent the bands of GST-H₂A (41.27 kDa) or GST-H₂B (42.82 kDa). (B) Visualization of the MoNap1-H₂A interaction using a BiFC assay. YFP signals were observed in vegetative hyphae in the transformant harboring MoNap1-YFP^{CTF} and YFP^{NTF}-H₂A. No detectable YFP signals were observed in the negative control transformants harboring MoNap1-YFP^{CTF} and YFP^{NTF} or YFP^{CTF} and YFP^{NTF}-H₂A. (C) Pull-down results between FLAG-MoNap1 and GST-Cyc1. FLAG-MoNap1 was detected in the GST-Cyc1 eluent but not in the GST eluent.

2.7. The NES of MoNap1 Is Dispensable for Localization and Binding the Histone Core Proteins H₂A and H₂B but Required for Growth and Pathogenicity

In both yeast and *Drosophila*, Nap1 has been reported to be a nucleocytoplasmic shuttling protein. However, in *M. oryzae*, MoNap1 mainly localized in the cytoplasm of conidial, appressorial, and hyphal cells (Figure 9A). Additionally, the treatment with leptomycin B (LMB, a specific nuclear export inhibitor) [34] did not result in the obviously increased accumulation of Nap1-GFP in the nucleus (Figure 9B).

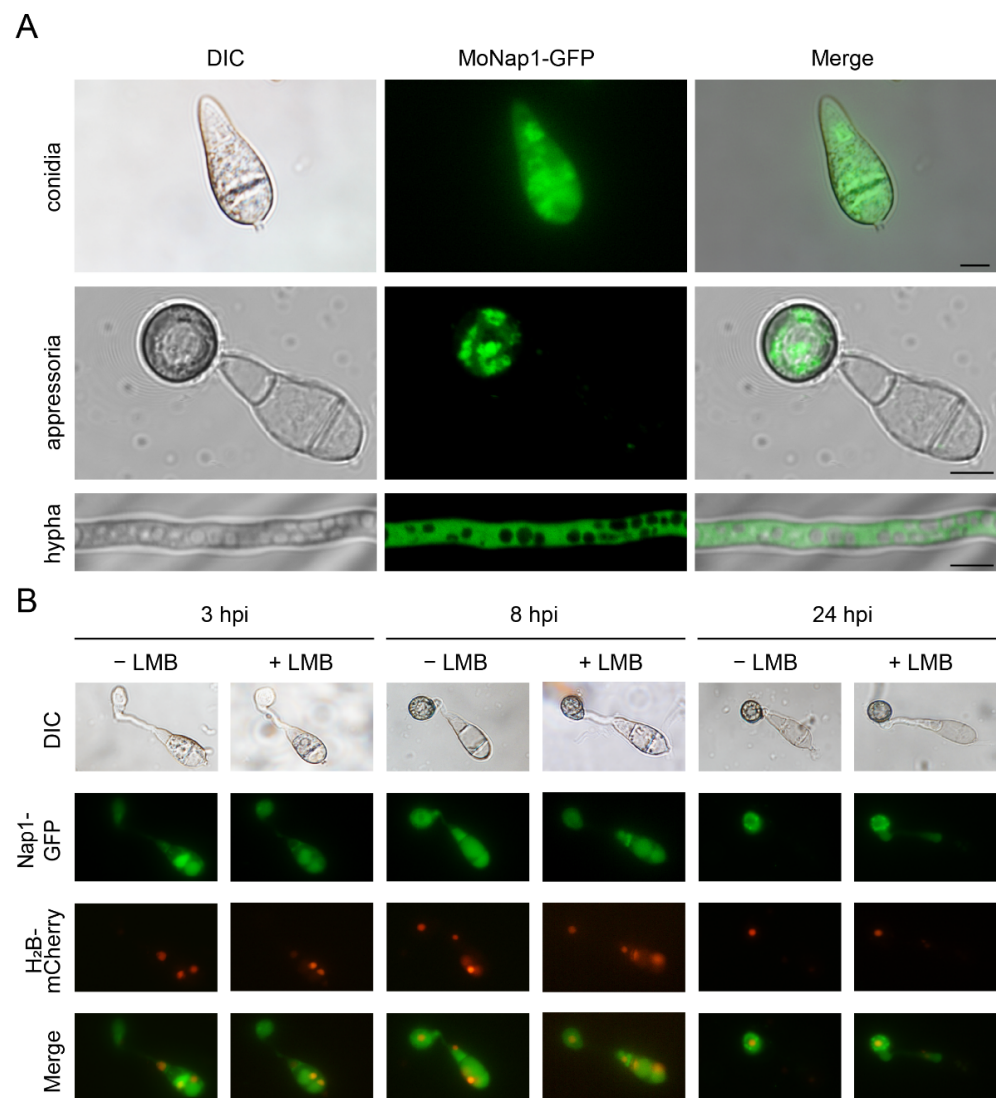


Figure 9. Subcellular localization of MoNap1 in *M. oryzae*. **(A)** Fluorescence signals of MoNap1-GFP in conidial, appressorial and hyphal cells. Bar, 5 μ m. **(B)** Fluorescence signals of MoNap1-GFP and H₂B-mCherry under LMB treatment in conidia and appressoria. Bar, 5 μ m.

In yeast, Nap1 shuttles via a leucine-rich NES [20], and this short peptide sequence is conserved in many species, including nematode Nap1 (nNap1), *Drosophila* Nap1 (dNap1), and human Nap1 (hNap1). MoNap1 contains a 16-amino acid sequence in the N-terminal region that is similar to the NES of the yeast Nap1 protein (Figure 10A). To investigate whether these sequences function as active NES signals, we constructed mutated Nap1 ^{Δ NES} in which Nap1 lacked the corresponding NES region. However, the deletion of the NES sequence in MoNap1-GFP (MoNap1 ^{Δ NES}-GFP) did not make Nap1 preferentially localize in the nucleus (Figure 10B).

We examined the possible relationship between histone binding and the NES sequence of Nap1. Therefore, we performed GST pull-down assays with FLAG-MoNap1 ^{Δ NES} and core histones. We found that MoNap1 ^{Δ NES} bound core histones similar to MoNap1 (Figure 10C). Therefore, the NES region is not involved in H₂A/H₂B binding.

Nevertheless, we found that *Monap1* ^{Δ NES} exhibited a phenotype similar to that of Δ *Monap1*, including reduced growth and virulence (Figure 10D–F).

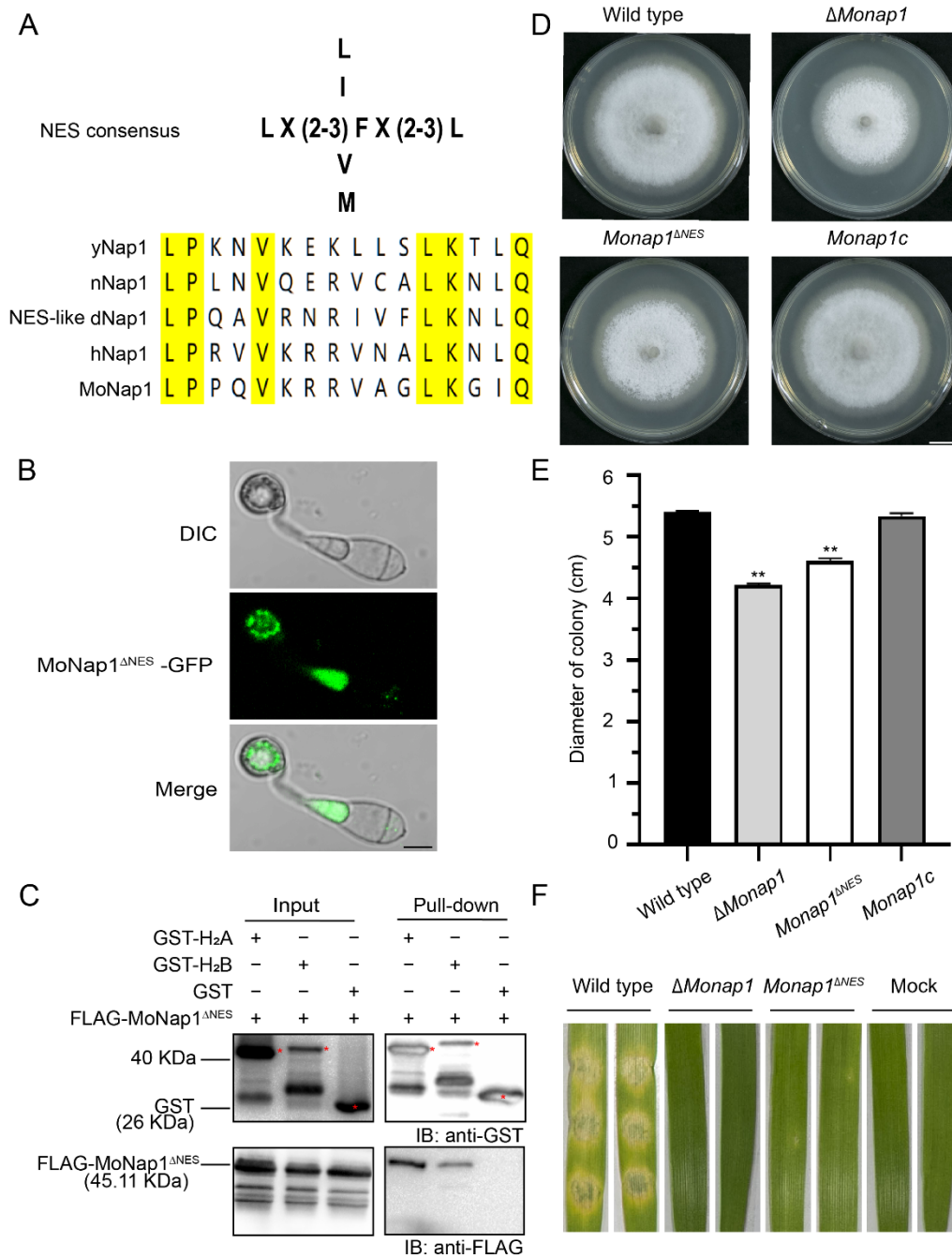


Figure 10. The NES region is not involved in H₂A/H₂B binding but is indispensable for growth and pathogenicity. **(A)** NES-like sequences of NAP1. The NES-like sequences of yeast Nap1 (yNap1), nematode Nap1 (nNap1), *Drosophila* Nap1 (dNap1), human Nap1 (hNap1) and MoNap1 are aligned. Yellow highlights indicate conserved amino acids. **(B)** Fluorescence signals of MoNap1^{ΔNES}-GFP in appressoria. Bar, 5 μ m. **(C)** Pull-down results between FLAG-MoNap1^{ΔNES} and GST-H₂A and GST-H₂B in *E. coli* BL21. FLAG-MoNap1^{ΔNES} was detected in GST-H₂A and GST-H₂B eluents but not in GST eluents. Red asterisks represent the bands of GST-H₂A (41.27 kDa), GST-H₂B (41.82 kDa), and GST (26 kDa). **(D)** Colonies of the wild type and Monap1^{ΔNES}. Bar, 1 cm. **(E)** Mycelial growth (cm) of the wild type and Monap1^{ΔNES} colonies. *n* = 5 independent biological replicates. Error bars represent the standard deviations. The data were analyzed by GraphPad Prism 8.0 and significant differences compared with the wild type were estimated by multiple *t* tests: ** *p* < 0.01. **(F)** Disease symptoms of leaf explants of barley inoculated with mycelial plugs from the wild-type and Monap1^{ΔNES} strains. The pictures were photographed at 4 dpi.

3. Discussion

Nap1 is a well-conserved protein in eukaryotes, such as mammals, *Drosophila*, and yeast; however, its roles in filamentous fungi are not well understood. *M. oryzae*, an important plant pathogenic fungus, is often used as a model organism in investigating pathogenic fungal-host molecular interactions. In this study, we characterized the biological roles of Nap1 in *M. oryzae* by knocking out *NAP1* and found that Nap1 plays diversified roles in aerial hyphal development, conidiophore and spore differentiation, appressorium formation, and virulence. *NAP1* in *S. cerevisiae* can eliminate the defects in the sporulation and virulence of the Δ *Monap1* mutant, suggesting that Nap1s in *M. oryzae* and *S. cerevisiae* are homologous in both biological function and protein sequence.

In *M. oryzae*, Δ *Monap1* displayed reduced spore production, abnormal appressoria, and decreased infection growth and virulence. The reduced conidiation in Δ *Monap1* is due to its fewer conidiophores and fewer spore numbers on each conidiophore. In *M. oryzae*, several transcription factor genes (*COS1*, *CONX2*, *MSTU1*, *GTA1*, *GCC1*, *FLBC*, *HOX2*, and *CON7*) [35–37] and autophagy genes, such as *ATG5* [38] and *TEA4* [39], are involved in the regulation of sporulation. The mRNA levels of two genes, *FLBC* and *CON7*, were significantly downregulated, suggesting a possible pathway regulating conidiation via *FLBC* and *CON7*. In addition, melanin promotes sporulation in the wild type 70–15 [40]. The lower melanin contents in the aerial hyphae of Δ *Monap1* are also responsible for its reduced spore production. *M. oryzae* penetrates the rice cell wall by a melanized, dome-shaped appressorium with a large turgor. In Δ *Monap1*, the appressorium morphology is abnormal and smaller than that in the wild type. Normal appressorium function depends on the microtubule arrangement and F-actin polymerization organized by septin [41]. The septin ring determines the polarity of the appressorium, which is required for plant penetration [42]. Septin GTPases can regulate the organization and functions of microtubule [43]. Moreover, in mammals, the stability of septin disks is dependent on intact microtubules [44]. In *C. albicans*, Nap1 is associated with the assembly of septin rings, and *NAP1* deletion leads to changes in septin dynamics [18]. In tobacco, Nap1 colocalizes with the mitotic spindle and the phragmoplast [12] and interacts with tubulins [32]. Benomyl, a microtubule inhibitor, destabilized microtubules in cells [45]. In *M. oryzae*, the deletion of *MoNAP1* led to increased resistance to benomyl and an increased proportion of abnormal appressoria, suggesting its function in microtubule arrangement. Abnormal cytoskeleton and appressorium morphology cause an abnormal septin ring [30,46]. Δ *Monap1* showed an abnormal distribution of Sep3 and Sep5 at the bottom of the appressorium at 24 hpi. This finding is consistent with the aberrant appressorium morphology of Δ *Monap1*. Thus, the reduced virulence of Δ *Monap1* may be the result of an abnormal appressorium morphology, which is probably related to the altered microtubule dynamics.

A dramatic change in microtubule dynamics occurs when cells enter mitosis. Spindle orientation is a microtubule-dependent process during mitosis that determines the division plane. Mitosis is induced specifically by kinase complexes that contain B-type cyclins and a cyclin-dependent kinase [19]. In yeast, Nap1 interacts with the B-type cyclin Clb2, which is involved in the assembly of the mitotic spindle. Nap1 is required for the ability of Clb2 to suppress polarized bud growth. In *M. oryzae*, Nap1 interacts with the B-type cyclin Cyc1. The deletion of *NAP1* alters the effect of benomyl on microtubule stability and alters microtubule stability during mitosis. In budding yeast, when the wild-type cells were cultured in media containing 11 $\mu\text{g mL}^{-1}$ benomyl, the cells were unable to assemble a functional mitotic spindle. However, Δ *nap1* cells do not exhibit a benomyl-induced mitotic delay [19]. This finding indicates that the deletion of *NAP1* either increases microtubule stability or reduces the requirements for microtubule function during mitosis. In *M. oryzae*, when conidia are treated with HU, a DNA replication inhibitor, the cells are arrested at the S phase, and appressorium formation is blocked [29,33]. We found that Δ *Monap1* also had an increased resistance to HU. Temperature is one of the key factors affecting division of cells, and high temperature inhibits the cell cycle in *Chlamydomonas reinhardtii* [47]. In *A. nidulans*, the *NimA* gene encodes a protein kinase necessary for mitosis [48]. An equivalent gene

mutant *MonimA*^{E37G} in *M. oryzae* grew normally at 26 °C but showed a reversible growth defect at 32 °C [49]. However, Δ *Monap1* exhibited a higher relative growth rate at 32 °C. Therefore, it is possible that MoNap1 is involved in the regulation of mitosis in *M. oryzae*.

Chitin [(1-4)- β -linked N-acetylglucosamine] is a major structural cell wall component in ascomycetes, and most chitin is fully acetylated and associated with (1-3)- β -glucan and (1-6)- β -glucan [50,51]. In this study, Δ *Monap1* was sensitive to two chitin-binding anionic dyes, CFW and CR, which inhibited the assembly of enzymes that connect chitin to (1-3)- β -glucan and (1-6)- β -glucan [52], indicating that the loss of *MoNAP1* affects the CWI pathway. The CWI pathway controls the cellular remodeling process in response to environmental challenges in fungi [28,52]. Bleomycin (BLM) is a DNA-damaging agent that acts by not only inducing DNA strand breaks [53] but also destroying cell wall components through oxidation and preventing the formation of fungal septum and cytokinesis [54–56]. The *nrp1-1 nrp2-1* mutant plants were significantly more sensitive to the bleomycin treatment and increased levels of DNA damage than the wild-type plants in *Arabidopsis* [57]. Conversely, our results showed that Δ *Monap1* increased resistance to BLM. The difference in the response to BLM may be due to the differences in nucleus and cell wall components or the differences in action sites of BLM between *Arabidopsis* and *M. oryzae*.

The localization of Nap1 in the cell has been an interesting issue, and Nap1 exhibits nucleocytoplasmic shuttling in many species. The distinct subcellular localization of Nap1 in the cell reflects functional diversity and complexity. Nap1 is a nucleocytoplasmic shuttling protein in yeast that is primarily localized in the cytoplasm at the steady state but localized in the nucleus when a leucine-rich nuclear export sequence (NES) is mutated [20]. Nap1 binds histone H₂A/H₂B dimers in the cytoplasm and participates in the import of histones into the nucleus [58]. The analysis of Nap1 phosphorylation revealed that Nap1 is phosphorylated at 11 sites in vivo in *S. cerevisiae* [59]. In vitro, Nap1 is a substrate for the phosphorylation of CK2 at three serines. Normal S-phase progression requires the reversible phosphorylation of Nap1, and the phosphorylation of Nap1 by CK2 appears to facilitate its import into the nucleus [59]. However, we did not observe increased nuclear localization of MoNap1 after deleting a putative NES, which is consistent with the observation in *C. albicans*, where the deletion of the NES also did not result in NAP1 accumulation in the nucleus [18]. Interestingly, in the BiFC assay, we found that the fluorescent signal was also mainly concentrated in the cytoplasm, which may be related to the fact that NAP1 binds histones in the cytoplasm to form a complex and participates in histone import into the nucleus [60].

In summary, we characterized the roles of Nap1, nucleosome assembly protein 1, in *M. oryzae* by molecular genetic assays and found that *MoNAP1* is required for fungal development and virulence probably through its involvement in microtubule dynamics.

4. Materials and Methods

4.1. Strains and Culture Conditions

Magnaporthe oryzae wild-type strain 70-15 (a strain artificially crossed in the laboratory) and the Δ *Monap1* mutant, the complementary strain of Δ *Monap1* (*Monap1c*), were cultured in complete medium (CM) or minimal medium (MM) at 25 °C under a 16 h light and 8 h dark cycle [61]. For the stress tests, the strains were cultured in CM supplemented with 0.004% sodium dodecyl sulfate (SDS), 75 μ g mL⁻¹ calcofluor white (CFW), 600 μ g mL⁻¹ Congo red (CR), 35 μ g mL⁻¹ bleomycin (BLM), 15 μ g mL⁻¹ benomyl, or 2 mM hydroxyurea (HU) at 25 °C in darkness for 9 d. For the temperature-sensitive stresses, the strains were cultured in CM at 32 °C under a 16 h light and 8 h dark cycle for 9 days.

4.2. Knockout of NAP1 in *M. oryzae*

An upstream fragment and a downstream fragment of *NAP1* from *M. oryzae* genomic DNA were amplified with the primers Up-F/Up-R and Down-F/Down-R, respectively. The primers used in this study are listed in Supplementary Table S1. A hygromycin B resistance gene, *HPH*, was cloned using the primers HPH-F and HPH-R. Three DNA fragments were

fused into a knockout cassette in *Hind*III- and *Xba*I-digested pKO3B [62] using a fusion enzyme (Vazyme, Nanjing, China). Then, the knockout cassette was transformed into the wild-type strain via *Agrobacterium tumefaciens*-mediated transformation (ATMT), and the null mutants were confirmed using a previously reported method [36,62]. First, the transformants were screened in selective CM containing 0.5 μ M 5-fluoro-2'-deoxyuridine (F2dU) and 200 μ g mL⁻¹ hygromycin B. Second, the genomic DNA of the transformants was isolated using an improved CTAB method. Then, the null mutants were identified using double PCR in which *MoNAP1* was amplified using the primer set S-F/S-R with β -*TUBULIN* (primers: Tbl-gF/Tbl-gR) as a positive control. The successful recombination of *HPH* into the deleted *MoNAP1* site was confirmed by another PCR using the primer set L-F/HPH-CKR. Third, the insertion copy number of *HPH* in the mutant genome was determined by quantitative real-time PCR (qPCR) using β -*TUBULIN* as a control (primer sets qHPH-F/qHPH-R and qtub-F/qtub-R).

For the complementary strain *Monap1c*, a 3.68 kb native full *NAP1* gene containing a promoter, coding sequence (CDS), and a terminator was cloned from *M. oryzae* wild-type genomic DNA by the primer set NAP1c-F/NAP1c-R and inserted into the *Eco*RI and *Xba*I-linearized vector pKD3, which contains a bialaphos resistance gene (*BAR*) [63]. The complemented DNA fragment was transformed into Δ *Monap1* via ATMT, and the transformants were selected in selection medium containing 750 μ g mL⁻¹ glufosinate ammonium. The expression of *MoNAP1* in the complementation strains was confirmed at the mRNA level by reverse transcription polymerase chain reaction (RT-PCR). To build a mutated *MoNAP1* in which the NES sequence was deleted (*MoNAP1* ^{Δ NES}), two segments (NAP1^{1–430} bp and NAP1^{478–1549} bp) with primers (NAP1 ^{Δ NES}-F1/NAP1 ^{Δ NES}-R1 and NAP1 ^{Δ NES}-F2/NAP1 ^{Δ NES}-R2) were amplified in the genomic DNA of *M. oryzae*, fused to the *Bam*HI-*Xba*I site of pKD3, and then transformed into Δ *Monap1* via ATMT. To complement the *NAP1* of *S. cerevisiae* into *M. oryzae*, a 2.35 kb *NAP1* gene was cloned from *S. cerevisiae* genomic DNA using the primer set yNAP1-F/yNAP1-R and inserted into the *Bam*HI and *Xba*I-linearized vector pKD5, which contains a sulfonyleurea resistance gene (*SUR*) [63]. The resulting construct was transformed into Δ *Monap1* by ATMT.

4.3. Phenotypic Characterization

The mutant phenotype was assayed according to previous reports [64,65]. To compare mycelial growth, a 5-mm agar block of 8-day-old wild type, Δ *Monap1*, and complementation strain *Monap1c* were inoculated in 7-cm plates containing 17.5 mL CM and cultured at 25 °C with a 16 h light and 8 h dark phase. The colony diameter was measured, and the colonies were photographed 9 days post-inoculation (dpi). Regarding sporulation, conidia were collected from 9-cm plates containing 30 mL CM at 12 dpi and counted with a counting chamber. Regarding conidiophore development, media containing vegetative hyphae were sliced into slender pieces and recultured under continuous light at 25 °C for 24 h [65]. To measure conidial germination and appressorium formation, 25 μ L of spore suspension (1×10^5 conidia mL⁻¹) were dropped on plastic coverslips and incubated at 22 °C under dark conditions. Conidial germination and appressorium formation were observed at 4 hpi and 24 hpi, respectively.

For the mycelial virulence assays, 5-mm mycelial pellets were inoculated on excised leaves of 7-day-old barley (*Hordeum vulgare*) for 4 days. The virulence assays of rice seedlings (*Oryza sativa* cultivar CO39) were performed by spraying spore suspensions (5×10^4 conidia mL⁻¹) in 0.2% (*w/v*) gelatin on 14-day-old rice seedlings. The rice seedlings were cultured in a wet container under dark conditions at 22 °C for 48 h and then recultured under a 16 h light and 8 h dark cycle at 25 °C for 3 days. To assess the disease lesion severity (disease score), the area of a 5-cm-long leaf with the most serious disease lesions in each seedling was counted [65]. Regarding host penetration, 20 μ L of spore suspensions (5×10^4 conidia mL⁻¹) of the wild-type, Δ *Monap1*, and *Monap1c* strains were dropped onto 7-day-old barley leaves and cultured at 25 °C. At 24 hpi, 36 hpi, and 48 hpi, the leaves

were collected, decolorized by methanol, fixed in alcoholic lactophenol, and observed under a microscope [64].

4.4. Observation of Fluorescence Fusion Proteins in *M. oryzae*

The fluorescence fusion protein Nap1-GFP was constructed by cloning a 1.5-kb *NAP1* via PCR with a primer set (NAP1-GFP-F/NAP1-GFP-R) from the wild-type genomic DNA and fused with GFP in the *Bam*HI and *Sma*I sites of pKD3-GFP [46]. To express Nap1^{ΔNES}-GFP, two segments (*NAP1*^{1–430 bp} and *NAP1*^{478–1549 bp}) of the *NAP1* coding sequence were amplified from the genome with primers (NAP1^{ΔNES}-GFP-F1/NAP1^{ΔNES}-GFP-R1 and NAP1^{ΔNES}-GFP-F2/NAP1^{ΔNES}-GFP-R2) and fused together with GFP in the pKD3 vector digested with *Xba*I. The fluorescent fusion protein expression vector was transformed into *ΔMonap1* via ATMT. The fluorescence signals were observed under a laser scanning confocal microscope (FV3000). To observe the effects of LMB on the localization of Nap1, 20 nM LMB were added to the conidial suspension, and the fluorescence signals were observed at 3 hpi, 8 hpi, and 24 hpi. To localize Sep3 and Sep5 in the wild type and *ΔMonap1* mutant, the vectors pKD5-Sep3-GFP and pKD5-Sep5-GFP into which *SEP3* or *SEP5* was inserted into the pKD5-GFP vector were transformed into the wild type and *ΔMonap1*, respectively [46].

4.5. Pull-Down Assays and Bimolecular Fluorescence Complementation (BiFC) Assay

For the pull-down assays, the cDNA fragments of *MoNAP1* and *MoNAP1*^{ΔNES} were inserted into pET21 containing a 3 × FLAG tag, and the cDNA fragments of *H2A*, *H2B*, and *CYC1* were inserted into pGEX-4T containing a GST tag. The expression vectors were transformed into *Escherichia coli* BL21 separately. FLAG-MoNap1 (46.85 kDa), FLAG-MoNap1^{ΔNES} (45.11 kDa), GST-H₂A (41.27 kDa), GST-H₂B (41.82 kDa), GST-Cyc1 (81.73 kDa), and GST (26 kDa) were expressed by induction using 0.2 M IPTG for 16 h and pulled down by GST beads C600913 (BBI, Shanghai, China). The proteins were separated by a Western blot assay and detected by an anti-GST antibody EM80701 (HUABIO, Hangzhou, China) or an anti-FLAG antibody M1403-2 (HUABIO, Hangzhou, China).

A BiFC analysis was used to observe the protein-protein interactions *in vivo* in *M. oryzae*. The plasmids used in the BiFC assay were constructed as previously described [66]. In brief, a *TUBULIN* promoter and a C-terminal fragment spanning approximately amino acids 155 to 238 of YFP (YFP^{CTF}) were inserted into the vector pKD9-HPH to form the plasmid pKD9-YFP^{CTF}-HPH. The plasmid pKD9-YFP^{CTF}-HPH was digested with *Bam*HI and *Sma*I and then ligated with the *MoNAP1* fragment amplified with a primer pair (NAP1-YFP^{CTF}-F/NAP1-YFP^{CTF}-R), resulting in the final pKD9-MoNAP1-YFP^{CTF}-HPH plasmid. Another N-terminal fragment spanning approximately amino acids 1 to 154 of YFP (YFP^{NTF}) was inserted into the vector pKD5-SUR and a *TUBULIN* promoter to form the plasmid pKD5-YFP^{NTF}-SUR. The plasmid pKD5-YFP^{NTF}-SUR was digested with *Sal*II and then ligated with the H₂A fragment amplified with a primer pair (H₂A-YFP^{NTF}-F/H₂A-YFP^{NTF}-R), resulting in the final pKD5-YFP^{NTF}-H₂A-SUR plasmid. Next, the pKD9-MoNAP1-YFP^{CTF}-HPH fusion vector was transformed into the 70-15 strain in combination with pKD5-YFP^{NTF}-H₂A-SUR. The transformants were screened in CM containing hygromycin B and sulfonyleurea, and at least three independent transformants were examined under an LSM710nlo laser scanning confocal microscope (Zeiss, Jena, Germany).

Supplementary Materials: The following supporting information can be downloaded at: <https://www.mdpi.com/article/10.3390/ijms23147662/s1>.

Author Contributions: Conceptualization, J.L. and Q.W.; investigation, J.W., P.H., Z.H. and Y.L.; data curation, Q.W.; writing—original draft preparation, Q.W.; writing—review and editing, J.L. and Q.W.; visualization, Q.W., J.W., P.H., Z.H. and Y.L.; supervision, J.L. and X.L.; project administration, J.L. and X.L.; funding acquisition, J.L., X.L. and F.L. All authors have read and agreed to the published version of the manuscript.

Funding: This work was funded by the Key R&D projects of Zhejiang Province (grant no. 2021C02010) and the National Natural Science Foundation of China (grant nos. 31871908). This work was also supported by a grant Organism Interaction from Zhejiang Xianghu Laboratory to FCL.

Institutional Review Board Statement: Not applicable.

Informed Consent Statement: Not applicable.

Data Availability Statement: All data supporting the findings of the current study are available within figures and supporting information. All strains generated during this study are available from the corresponding author upon reasonable request.

Acknowledgments: We thank Xiaoxiao Feng at Agricultural Experiment Station, Zhejiang University for her help in experiment management.

Conflicts of Interest: The authors declare no conflict of interest.

References

1. Talbot, N.J. On the Trail of a Cereal Killer: Exploring the Biology of *Magnaporthe grisea*. *Annu. Rev. Microbiol.* **2003**, *57*, 177–202. [[CrossRef](#)]
2. Hamer, J.E.; Talbot, N.J. Infection-related development in the rice blast fungus *Magnaporthe grisea*. *Curr. Opin. Microbiol.* **1998**, *1*, 693–697. [[CrossRef](#)]
3. Hamer, J.E.; Howard, R.J.; Chumley, F.G.; Valent, B. A Mechanism for Surface Attachment in Spores of a Plant Pathogenic Fungus. *Science* **1988**, *239*, 288–290. [[CrossRef](#)]
4. De Jong, J.C.; McCormack, B.J.; Smirnoff, N.; Talbot, N.J. Glycerol generates turgor in rice blast. *Nature* **1997**, *389*, 244–245. [[CrossRef](#)]
5. Gupta, L.; Vermani, M.; Ahluwalia, S.K.; Vijayaraghavan, P. Molecular virulence determinants of *Magnaporthe oryzae*: Disease pathogenesis and recent interventions for disease management in rice plant. *Mycology* **2021**, *12*, 174–187. [[CrossRef](#)]
6. Ishimi, Y.; Kojima, M.; Yamada, M.-A.; Hanaoka, F. Binding mode of nucleosome-assembly protein (AP-I) and histones. *Eur. J. Biochem.* **1987**, *162*, 19–24. [[CrossRef](#)]
7. Ishimi, Y.; Kikuchi, A. Identification and molecular cloning of yeast homolog of nucleosome assembly protein I which facilitates nucleosome assembly in vitro. *J. Biol. Chem.* **1991**, *266*, 7025–7029. [[CrossRef](#)]
8. Mindrinos, M.; Katagiri, F.; Yu, G.-L.; Ausubel, F.M. The a-thaliana disease resistance gene RPS2 encodes a protein containing a nucleotide-binding site and leucine-rich repeats. *Cell* **1994**, *78*, 1089–1099. [[CrossRef](#)]
9. Yoon, H.W.; Kim, M.C.; Lee, S.Y.; Hwang, I.; Bahk, J.D.; Hong, J.C.; Ishimi, Y.; Cho, M.J. Molecular cloning and functional characterization of a cDNA encoding nucleosome assembly protein 1 (NAP-1) from soybean. *Mol. Gen. Genet.* **1995**, *249*, 465–473. [[CrossRef](#)]
10. Lankenau, S.; Barnickel, T.; Marhold, J.; Lyko, F.; Mechler, B.M.; Lankenau, D.-H. Knockout Targeting of the *Drosophila* *Nap1* Gene and Examination of DNA Repair Tracts in the Recombination Products. *Genetics* **2003**, *163*, 611–623. [[CrossRef](#)]
11. Rogner, U.C.; Spyropoulos, D.D.; Le Novère, N.; Changeux, J.-P.; Avner, P. Control of neurulation by the nucleosome assembly protein-1-like 2. *Nat. Genet.* **2000**, *25*, 431–435. [[CrossRef](#)]
12. Dong, A.; Zhu, Y.; Yu, Y.; Cao, K.; Sun, C.; Shen, W.-H. Regulation of biosynthesis and intracellular localization of rice and tobacco homologues of nucleosome assembly protein 1. *Planta* **2003**, *216*, 561–570. [[CrossRef](#)]
13. Ishimi, Y.; Hirosumi, J.; Sato, W.; Sugasawa, K.; Yokota, S.; Hanaoka, F.; Yamada, M.-A. Purification and initial characterization of a protein which facilitates assembly of nucleosome-like structure from mammalian cells. *JBIC J. Biol. Inorg. Chem.* **1984**, *142*, 431–439. [[CrossRef](#)]
14. Andrews, A.J.; Downing, G.; Brown, K.; Park, Y.-J.; Luger, K. A Thermodynamic Model for Nap1-Histone Interactions. *J. Biol. Chem.* **2008**, *283*, 32412–32418. [[CrossRef](#)]
15. Ohkuni, K.; Shirahige, K.; Kikuchi, A. Genome-wide expression analysis of NAP1 in *Saccharomyces cerevisiae*. *Biochem. Biophys. Res. Commun.* **2003**, *306*, 5–9. [[CrossRef](#)]
16. Altman, R.; Kellogg, D. Control of Mitotic Events by Nap1 and the Gin4 Kinase. *J. Cell Biol.* **1997**, *138*, 119–130. [[CrossRef](#)]
17. Asahara, H.; Tartare-Deckert, S.; Nakagawa, T.; Ikehara, T.; Hirose, F.; Hunter, T.; Ito, T.; Montminy, M. Dual Roles of p300 in Chromatin Assembly and Transcriptional Activation in Cooperation with Nucleosome Assembly Protein 1 In Vitro. *Mol. Cell. Biol.* **2002**, *22*, 2974–2983. [[CrossRef](#)]
18. Huang, Z.-X.; Zhao, P.; Zeng, G.; Wang, Y.-M.; Sudbery, I.; Wang, Y. Phosphoregulation of Nap1 Plays a Role in Septin Ring Dynamics and Morphogenesis in *Candida albicans*. *mBio* **2014**, *5*, e00915-13. [[CrossRef](#)]
19. Kellogg, D.R.; Murray, A.W. NAP1 acts with Clb2 to perform mitotic functions and to suppress polar bud growth in budding yeast. *J. Cell Biol.* **1995**, *130*, 675–685. [[CrossRef](#)]
20. Miyaji-Yamaguchi, M.; Kato, K.; Nakano, R.; Akashi, T.; Kikuchi, A.; Nagata, K. Involvement of Nucleocytoplasmic Shuttling of Yeast Nap1 in Mitotic Progression. *Mol. Cell. Biol.* **2003**, *23*, 6672–6684. [[CrossRef](#)]

21. Ito, T.; Bulger, M.; Kobayashi, R.; Kadonaga, J.T. Drosophila NAP-1 is a core histone chaperone that functions in ATP-facilitated assembly of regularly spaced nucleosomal arrays. *Mol. Cell. Biol.* **1996**, *16*, 3112–3124. [[CrossRef](#)]
22. Rodriguez, P.; Munro, D.; Prawitt, D.; Chu, L.L.; Bric, E.; Kima, J.; Reid, L.H.; Daviese, C.; Nakagama, H.; Loebbert, R.; et al. Functional Characterization of Human Nucleosome Assembly Protein-2 (NAP1L4) Suggests a Role as a Histone Chaperone. *Genomics* **1997**, *44*, 253–265. [[CrossRef](#)]
23. Fujii-Nakata, T.; Ishimi, Y.; Okuda, A.; Kikuchi, A. Functional analysis of nucleosome assembly protein, NAP-1. The negatively charged COOH-terminal region is not necessary for the intrinsic assembly activity. *J. Biol. Chem.* **1992**, *267*, 20980–20986. [[CrossRef](#)]
24. Li, M.; Strand, D.; Krehan, A.; Pyerin, W.; Heid, H.; Neumann, B.; Mechler, B.M. Casein kinase 2 binds and phosphorylates the nucleosome assembly protein-1 (NAP1) in *Drosophila melanogaster*. *J. Mol. Biol.* **1999**, *293*, 1067–1084. [[CrossRef](#)]
25. McQuibban, G.A.; Comisso-Cappelli, C.N.; Lewis, P.N. Assembly, Remodeling, and Histone Binding Capabilities of Yeast Nucleosome Assembly Protein 1. *J. Biol. Chem.* **1998**, *273*, 6582–6590. [[CrossRef](#)]
26. Lee, J.Y.; Lake, R.J.; Kirk, J.; Bohr, V.A.; Fan, H.-Y.; Hohng, S. NAP1L1 accelerates activation and decreases pausing to enhance nucleosome remodeling by CSB. *Nucleic Acids Res.* **2017**, *45*, 4696–4707. [[CrossRef](#)]
27. Grande, M.; Lambea, E.; Fajardo, A.; López-Avilés, S.; Kellogg, D.; Aligue, R. Crosstalk between Nap1 protein and Cds1 checkpoint kinase to maintain chromatin integrity. *Bba-Mol. Cell Res.* **2008**, *1783*, 1595–1604. [[CrossRef](#)]
28. Sun, L.; Qian, H.; Liu, M.; Wu, M.; Wei, Y.; Zhu, X.; Lu, J.; Lin, F.; Liu, X. Endosomal sorting complexes required for transport-0 (ESCRT-0) are essential for fungal development, pathogenicity, autophagy and ER-phagy in *Magnaporthe oryzae*. *Environ. Microbiol.* **2022**, *24*, 1076–1092. [[CrossRef](#)]
29. Osés-Ruiz, M.; Sakulkoo, W.; Littlejohn, G.R.; Martin-Urdiroz, M.; Talbot, N.J. Two independent S-phase checkpoints regulate appressorium-mediated plant infection by the rice blast fungus *Magnaporthe oryzae*. *Proc. Natl. Acad. Sci. USA* **2017**, *114*, E237–E244. [[CrossRef](#)]
30. Li, L.; Zhu, X.-M.; Su, Z.-Z.; Del Poeta, M.; Liu, X.-H.; Lin, F.-C. Insights of roles played by septins in pathogenic fungi. *Virulence* **2021**, *12*, 1550–1562. [[CrossRef](#)]
31. Aguilar-Gurrieri, C.; Larabi, A.; Vinayachandran, V.; Patel, N.A.; Yen, K.; Reja, R.; Ebong, I.; Schoehn, G.; Robinson, C.V.; Pugh, B.F.; et al. Structural evidence for Nap1-dependent H2A–H2B deposition and nucleosome assembly. *EMBO J.* **2016**, *35*, 1465–1482. [[CrossRef](#)]
32. Dong, A.; Liu, Z.; Zhu, Y.; Yu, F.; Li, Z.; Cao, K.; Shen, W.-H. Interacting Proteins and Differences in Nuclear Transport Reveal Specific Functions for the NAP1 Family Proteins in Plants. *Plant Physiol.* **2005**, *138*, 1446–1456. [[CrossRef](#)]
33. Osés-Ruiz, M.; Talbot, N.J. Cell cycle-dependent regulation of plant infection by the rice blast fungus *Magnaporthe oryzae*. *Commun. Integr. Biol.* **2017**, *10*, e1372067. [[CrossRef](#)]
34. Toyoshima, F.; Moriguchi, T.; Wada, A.; Fukuda, M.; Nishida, E. Nuclear export of cyclin B1 and its possible role in the DNA damage-induced G2 checkpoint. *EMBO J.* **1998**, *17*, 2728–2735. [[CrossRef](#)]
35. Odenbach, D.; Breth, B.; Thines, E.; Weber, R.W.S.; Anke, H.; Foster, A.J. The transcription factor Con7p is a central regulator of infection-related morphogenesis in the rice blast fungus *Magnaporthe grisea*. *Mol. Microbiol.* **2007**, *64*, 293–307. [[CrossRef](#)]
36. Lu, J.-P.; Cao, H.; Zhang, L.; Huang, P.; Lin, F. Systematic Analysis of Zn₂Cys₆ Transcription Factors Required for Development and Pathogenicity by High-Throughput Gene Knockout in the Rice Blast Fungus. *PLOS Pathog.* **2014**, *10*, e1004432. [[CrossRef](#)]
37. Qu, Y.; Wang, J.; Zhu, X.; Dong, B.; Liu, X.; Lu, J.; Lin, F. The P5-type ATPase Spf1 is required for development and virulence of the rice blast fungus *Pyricularia oryzae*. *Curr. Genet.* **2020**, *66*, 385–395. [[CrossRef](#)]
38. Lu, J.-P.; Liu, X.-H.; Feng, X.-X.; Min, H.; Lin, F.-C. An autophagy gene, MgATG5, is required for cell differentiation and pathogenesis in *Magnaporthe oryzae*. *Curr. Genet.* **2009**, *55*, 461–473. [[CrossRef](#)]
39. Patkar, R.N.; Suresh, A.; Naqvi, N.I. MoTea4-Mediated Polarized Growth Is Essential for Proper Asexual Development and Pathogenesis in *Magnaporthe oryzae*. *Eukaryot. Cell* **2010**, *9*, 1029–1038. [[CrossRef](#)]
40. Huang, P.; Cao, H.; Li, Y.; Zhu, S.; Wang, J.; Wang, Q.; Liu, X.; Lin, F.-C.; Lu, J. Melanin Promotes Spore Production in the Rice Blast Fungus *Magnaporthe oryzae*. *Front. Microbiol.* **2022**, *13*, 843838. [[CrossRef](#)]
41. Dulal, N.; Rogers, A.M.; Proko, R.; Bieger, B.D.; Liyanage, R.; Krishnamurthi, V.R.; Wang, Y.; Egan, M.J. Turgor-dependent and coronin-mediated F-actin dynamics drive septin disc-to-ring remodeling in the blast fungus *Magnaporthe oryzae*. *J. Cell Sci.* **2021**, *134*, jcs251298. [[CrossRef](#)]
42. Gupta, Y.K.; Dagdas, Y.F.; Martinez-Rocha, A.L.; Kershaw, M.J.; Littlejohn, G.R.; Ryder, L.S.; Sklenar, J.; Menke, F.; Talbot, N.J. Septin-Dependent Assembly of the Exocyst Is Essential for Plant Infection by *Magnaporthe oryzae*. *Plant Cell* **2015**, *27*, 3277–3289. [[CrossRef](#)]
43. Spiliotis, E.T. Regulation of microtubule organization and functions by septin GTPases. *Cytoskeleton* **2010**, *67*, 339–345. [[CrossRef](#)]
44. Sellin, M.E.; Holmfeldt, P.; Stenmark, S.; Gullberg, M. Microtubules support a disk-like septin arrangement at the plasma membrane of mammalian cells. *Mol. Biol. Cell* **2011**, *22*, 4588–4601. [[CrossRef](#)]
45. Hoyt, M.; Totis, L.; Roberts, B.S. *cerevisiae* genes required for cell cycle arrest in response to loss of microtubule function. *Cell* **1991**, *66*, 507–517. [[CrossRef](#)]
46. Qu, Y.; Cao, H.; Huang, P.; Wang, J.; Liu, X.; Lu, J.; Lin, F.-C. A kelch domain cell end protein, PoTea1, mediates cell polarization during appressorium morphogenesis in *Pyricularia oryzae*. *Microbiol. Res.* **2022**, *259*, 126999. [[CrossRef](#)]

47. Zachleder, V.; Ivanov, I.; Vítová, M.; Bišová, K. Cell Cycle Arrest by Supraoptimal Temperature in the Alga *Chlamydomonas reinhardtii*. *Cells* **2019**, *8*, 1237. [[CrossRef](#)]
48. Osmani, S.A.; Engle, D.B.; Doonan, J.; Morris, N. Spindle formation and chromatin condensation in cells blocked at interphase by mutation of a negative cell cycle control gene. *Cell* **1988**, *52*, 241–251. [[CrossRef](#)]
49. Saunders, D.G.; Aves, S.J.; Talbot, N.J. Cell Cycle–Mediated Regulation of Plant Infection by the Rice Blast Fungus. *Plant Cell* **2010**, *22*, 497–507. [[CrossRef](#)]
50. Wessels, J.G.H. Developmental regulation of fungal cell wall formation. *Annu. Rev. Phytopathol.* **1994**, *32*, 413–437. [[CrossRef](#)]
51. Sun, D.; Cao, H.; Shi, Y.; Huang, P.; Dong, B.; Liu, X.; Lin, F.; Lu, J. The regulatory factor X protein MoRfx1 is required for development and pathogenicity in the rice blast fungus *Magnaporthe oryzae*. *Mol. Plant Pathol.* **2017**, *18*, 1075–1088. [[CrossRef](#)]
52. Ram, A.F.J.; Klis, F.M. Identification of fungal cell wall mutants using susceptibility assays based on Calcofluor white and Congo red. *Nat. Protoc.* **2006**, *1*, 2253–2256. [[CrossRef](#)]
53. Hecht, S.M. Bleomycin: New Perspectives on the Mechanism of Action. *J. Nat. Prod.* **2000**, *63*, 158–168. [[CrossRef](#)]
54. Beaudouin, R.; Lim, S.T.; Steide, J.A.; Powell, M.; McKoy, J.; Pramanik, A.J.; Johnson, E.; Moore, C.W.; Lipke, P.N. Bleomycin affects cell wall anchorage of mannoproteins in *Saccharomyces cerevisiae*. *Antimicrob. Agents Chemother.* **1993**, *37*, 1264–1269. [[CrossRef](#)]
55. Lim, S.T.; Jue, C.K.; Moore, C.W.; Lipke, P. Oxidative cell wall damage mediated by bleomycin-Fe(II) in *Saccharomyces cerevisiae*. *J. Bacteriol.* **1995**, *177*, 3534–3539. [[CrossRef](#)]
56. Moore, C.W.; McKoy, J.; Del Valle, R.; Armstrong, D.; Bernard, E.M.; Katz, N.; Gordon, R.E. Fungal Cell Wall Septation and Cytokinesis Are Inhibited by Bleomycins. *Antimicrob. Agents Chemother.* **2003**, *47*, 3281–3289. [[CrossRef](#)]
57. Zhu, Y.; Dong, A.; Meyer, D.; Pichon, O.; Renou, J.-P.; Cao, K.; Shen, W.-H. *Arabidopsis* NRP1 and NRP2 Encode Histone Chaperones and Are Required for Maintaining Postembryonic Root Growth. *Plant Cell* **2006**, *18*, 2879–2892. [[CrossRef](#)]
58. Mosammaparast, N.; Ewart, C.S.; Pemberton, L.F. A role for nucleosome assembly protein 1 in the nuclear transport of histones H2A and H2B. *EMBO J.* **2002**, *21*, 6527–6538. [[CrossRef](#)]
59. Calvert, M.E.K.; Keck, K.M.; Ptak, C.; Shabanowitz, J.; Hunt, D.F.; Pemberton, L.F. Phosphorylation by Casein Kinase 2 Regulates Nap1 Localization and Function. *Mol. Cell. Biol.* **2008**, *28*, 1313–1325. [[CrossRef](#)]
60. Mosammaparast, N.; Jackson, K.R.; Guo, Y.; Brame, C.J.; Shabanowitz, J.; Hunt, D.F.; Pemberton, L.F. Nuclear Import of Histone H2a and H2b Is Mediated by a Network of Karyopherins. *J. Cell Biol.* **2001**, *153*, 251–262. [[CrossRef](#)]
61. Talbot, N.J.; Ebbole, D.J.; Hamer, J.E. Identification and characterization of MPG1, a gene involved in pathogenicity from the rice blast fungus *Magnaporthe grisea*. *Plant Cell* **1993**, *5*, 1575–1590. [[CrossRef](#)] [[PubMed](#)]
62. Yan, Y.; Wang, H.; Zhu, S.; Wang, J.; Liu, X.; Lin, F.; Lu, J. The Methylcitrate Cycle Is Required for Development and Virulence in the Rice Blast Fungus *Pyricularia oryzae*. *Mol. Plant-Microbe Interact.* **2019**, *32*, 1148–1161. [[CrossRef](#)] [[PubMed](#)]
63. Zhu, S.; Yan, Y.; Qu, Y.; Wang, J.; Feng, X.; Liu, X.; Lin, F.; Lu, J. Role refinement of melanin synthesis genes by gene knockout reveals their functional diversity in *Pyricularia oryzae* strains. *Microbiol. Res.* **2020**, *242*, 126620. [[CrossRef](#)] [[PubMed](#)]
64. Lu, J.-P.; Feng, X.-X.; Liu, X.-H.; Lu, Q.; Wang, H.-K.; Lin, F.-C. Mnh6, a nonhistone protein, is required for fungal development and pathogenicity of *Magnaporthe grisea*. *Fungal Genet. Biol.* **2007**, *44*, 819–829. [[CrossRef](#)]
65. Cao, H.; Huang, P.; Zhang, L.; Shi, Y.; Sun, D.; Yan, Y.; Liu, X.; Dong, B.; Chen, G.; Snyder, J.H.; et al. Characterization of 47 Cys₂-His₂ zinc finger proteins required for the development and pathogenicity of the rice blast fungus *Magnaporthe oryzae*. *New Phytol.* **2016**, *211*, 1035–1051. [[CrossRef](#)] [[PubMed](#)]
66. Liu, T.-B.; Liu, X.-H.; Lu, J.-P.; Zhang, L.; Min, H.; Lin, F.-C. The cysteine protease MoAtg4 interacts with MoAtg8 and is required for differentiation and pathogenesis in *Magnaporthe oryzae*. *Autophagy* **2010**, *6*, 74–85. [[CrossRef](#)]